Hindawi
Shock and Vibration
Volume 2021, Article ID 6638009, 15 pages
https://doi.org/10.1155/2021/6638009

Research Article

Study on Occurrence Mechanism of Coal Pillar in L-Shaped Zone during Fully Mechanized Mining Period and Prevention Technology

Zeng-qiang Yang,[1,2] **Hong-mei Wang**,[1,3] **De-quan Sun**,[1,4] **Xian-jian Ma**,[1,3] **Ming-bao Xu**,[1,3] **and Nai-xin Si**[1,3]

[1]*Shandong Province Engineering Laboratory of Deep Mine Rockburst Disaster Assessment, Jinan, Shandong 250104, China*
[2]*School of Transportation Engineering, Jiangsu Vocational Institute of Architectural Technology, Xuzhou, Jiangsu 221116, China*
[3]*Shandong Province Research Institute of Coal Geology Planning and Exploration, Jinan, Shandong 250104, China*
[4]*The Four Prospecting Team of Shandong Coal Geology Bureau, Weifang, Shandong 150027, China*

Correspondence should be addressed to Zeng-qiang Yang; zengqiang5@126.com

Received 31 December 2020; Revised 14 January 2021; Accepted 19 January 2021; Published 9 February 2021

Academic Editor: Guangchao Zhang

In order to study the occurrence mechanism of rock burst in L-shaped zone during a fully mechanized mining period, the No. 705 working face which is located in Baojishan Colliery is taken as a typical engineering background. By means of in situ investigation, theoretical analysis, numerical simulation, in situ tests, and relevant monitoring methods, the occurrence mechanism of rock burst and corresponding prevention technology are studied. The results show that a coal pillar with some confining pressure in the L-shaped zone is established by FLAC^{3D} numerical simulation software, and the numerical simulation results indicate that the change in static load has a greater effect than dynamic load on coal pillar unstable failure; the static load plays a role in storing energy, and dynamic load plays a role in inducing rock burst; the bolt-mesh-cable support and high-pressure water jet unloading combined technology is put forward to prevent rock burst in roadways, and the numerical simulation results show that stress distribution of surrounding rock meets the model of strong-soft-strong (3S) structure, and the moment distribution is reasonable. In the follow-up mining, a limit value of coal fines is used to determine that this measure is a reasonable method to prevent rock burst. The study conclusions provide theoretical foundation and new guidance for preventing rock burst by synergistic effect technology in roadways.

1. Introduction

In recent years, with the popularity of fully mechanized mining hydraulic support and the improvement of supporting strength of working face, rock burst accidents appear mostly in the roadway. Research statistics showed that more than 75% of rock burst accidents occurred in the two tunnels of the working face, especially in the advance support range of 0~80 m of the working face [1–3]. Therefore, the research of antierosion of roadway with rock burst has become one of the important issues to be solved urgently.

At present, for two types of typical roadway rock burst of pressure type and shock (pressure) type, the phenomenon of dynamic and static combination-induced rock burst is generally accepted. Pan [4] proposed the initiation theory of roadway impact ground pressure based on microseismic monitoring results; He et al. [5] studied the mechanism of dynamic and static combination-induced impact ground pressure; Li et al. [6] established the damage criterion under the combined dynamic and static action of coal and rock bodies and analyzed the mechanical response characteristics of deep mine columns under the combined dynamic and static action; and Peng and Lu and Wen et al. [7, 8] studied the impact damage characteristics of the roadway by dynamic loads using numerical model simulations. In terms of

management technology, Dou et al. [9] put forward the theory of strength weakening and decompression of the coal-rock body and conducted in-depth research around deep hole blasting, large diameter drilling, coal seam high-pressure water injection, and other pressure relief techniques and equipment. Gao et al. [10] established a strong-weak-strong (3S) triple impact prevention mechanics model based on the impact vibration damage mechanism of the roadway. Kang et al. [11] believed that the impact manifestation of the roadway could be eliminated or attenuated by strong support and research on energy-absorbing support materials. Based on the mechanism of rock burst in roadway, the above studies have carried out special studies from the aspects of pressure relief prevention and support prevention, respectively, but few studies on the synergistic effect of roadway pressure relief and support have been involved.

In this paper, taking the frequent occurrence of impact at the end of the working face as the breakthrough point, the strain-softening constitutive model of FLAC^{3D} software is used to simulate and analyze the effect of static load and dynamic load on the failure and instability of coal pillar in an L-shaped area.

2. Engineering General Situations

2.1. Geological Overview of the Working Face. No. 705 working face is located in the east wing of the mine, the working face is now in the back mining, its upper No. 703 working face and No. 701 working face has been mined, and the lower part is the original coal seam of No. 707 working face. No. 705 fully mechanized top coal caving face is located in the +1090 m level of the mine, with an average mining depth of about 590 m. The upper part is bounded by the isolated coal pillar of No. 703 working face, the lower part is the original coal seam of No. 707 working face, and the mineable boundary of the minefield is the boundary in the east. The working face has a return air chute length of 665 m and a haulage gateway length of 680 m, with an average mineable strike length of 640 m and an average inclined length of 81 m. The small fault with 0.5~2 m drop in No. 705 working face is more developed, which constitutes a small local influence on the recovery, and the open cut is arranged to the west of F10 fault, which does not have enough influence on the recovery, while the drop of Fa fault in the west is larger, and the influence on the mining of working face becomes bigger gradually as the distance between the working face and it shortens.

No. 705 working face is mainly mining one coal seam with a single coal seam structure and stable coal thickness. The average coal thickness is 10.78 m, the average inclination angle is 26°, the capacity is 1.40 t/m^3, the solidity coefficient is 1.3~1.5, and comprehensive mining No. 705 comprehensive working face project plan location is shown in Figure 1.

The critical index values of burst potentiality about coal seam are shown in Table 1.

The average mining depth of one coal seam in the mine is about 590 m. The coal-rock samples are taken from the No. 705 working face and No. 706 haulage gateway to determine the laboratory physical and mechanical parameters. The determination contents include dynamic failure time (D_T), elastic energy index (W_{ET}), impact energy index (K_E), and uniaxial compressive strength (R_C) of coal samples. According to the measurement results of coal samples, it can be comprehensively evaluated that a coal seam in this mine has class III strong impact tendency (refer to Table 1). The determination results are shown in Table 2. The critical index values of burst potentiality about roof are shown in Table 3.

Within 40 m above the coal seam is a multilayered mudstone of varying thickness, taking the value mudstone with a maximum stratification thickness of 1 m. The overburden load per unit width (q), the single roof bending energy index (U_{WQ}), and thus the composite roof bending energy index (U_{WQS}) can be calculated from the results of rock sample measurements and the application of the corresponding equations. Since the U_{WQS} value is less than 120, refer to Table 3, and it is determined that the roof of a coal seam in this mine has a weak impact tendency of class II. The measured parameters and calculation results are shown in Table 4.

2.2. Analysis of the Occurrence and Causes of Shocks. During the driving period, the dynamic pressure of No. 705 fully mechanized caving face did not appear. As of November 2013, monitoring to No. 705 working face back mining process has occurred in the impact manifestation, there are 5 serious impact manifestations, and No. 705 working face advance location and impact ground pressure manifestation location distribution are shown in Figure 2.

From Figure 2, the following observations hold:

(1) The location of the impact appeared with the No. 705 fully mechanized caving face back mining regular dynamic forward and the location of the occurrence of more concentrated in the return to the wind down the slot.

(2) Among the 5 shocks, ①, ④, and ⑤ shocks were more serious.

As can be seen from Figure 2, the five severe impact manifestations that have occurred since June 26, 2013, when the No. 705 fully mechanized top coal caving face were opened for cut-hole retrieval, up to November 30 of that year. The "7.18" impact (①) appearing working face is located in the "first square" influence zone which means that the advanced distance is equal to the width of mining face, affected by the large area of the roof activity; the "9.10" impact (②) appearances are expected to be influenced by the superimposed effect of the lateral support pressure formed in the adjacent mining area; the "9.16" impact (③) appears to work face all bracket pressure increases and is expected to be as the work face advances, and the overlying rock activity in the mining area intensifies, a large area across the fall, fracture-induced incoming pressure; the "10.7" impact (④) revealed that the working face is in the position of the second sighting, and the working face is shut down for 6 days, affected by the mining disturbance of the resumed production of the working face and the large area of the roof

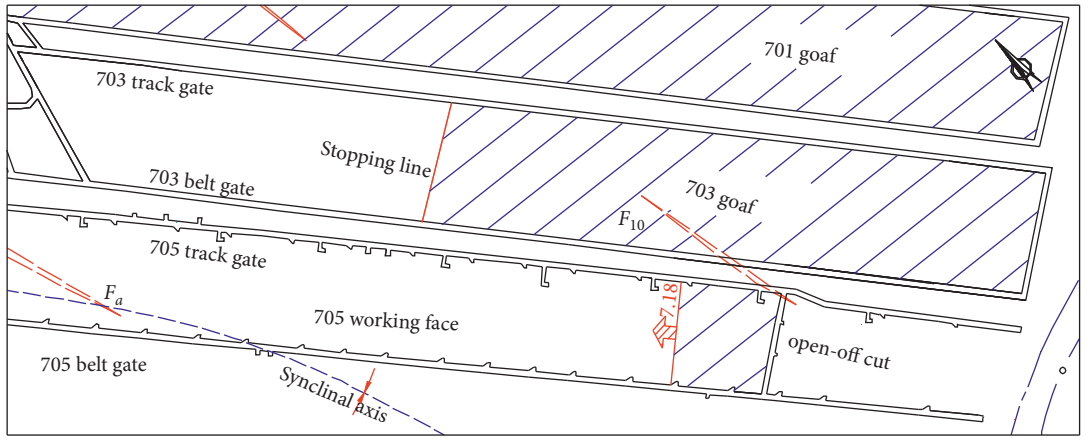

Figure 1: No. 705 fully mechanized working face layout.

Table 1: The critical index values of burst potentiality about coal seam.

Burst potentiality testing indexes				Burst potentiality degree	Classification
D_T/ms	W_{ET}	K_E	R_C (MPa)		
$D_T > 500$	$W_{ET} < 2$	$K_E < 1.5$	$R_C < 7$	No	I
$50 < D_T \leq 500$	$2 \leq W_{ET} < 5$	$1.5 \leq K_E < 5$	$7 \leq R_C < 14$	Weak	II
$D_T \leq 50$	$W_{ET} \geq 5$	$K_E \geq 5$	$R_C \geq 14$	Strong	III

Table 2: Testing result of #1 coal samples impact tendency.

Coal sample	Indexes				Impact tendency
	D_T	W_{ET}	K_E	R_c	
No. 3	29.4	4.259	10.428	27.118	Strong impact tendency (III)
	Strong	Weak	Strong	Strong	

Table 3: Critical index values of burst potentiality about roof and floor.

Burst potentiality testing indexes, U_{WQ} (kJ)	Burst potentiality degree	Classification
$U_{WQ} < 10$	No	I
$10 < U_{WQ} \leq 100$	Weak	II
$U_{WQ} > 100$	Strong	III

Table 4: Testing result of roof samples impact tendency.

Name	Indexes			Determination result
Roof	Tensile strength (MPa)	Density (g/cm^3)	Elasticity modulus (GPa)	Weak impact tendency (II)
	3.459	2.626	6.508	
	Thickness (m)	Overburden load (MPa)	Bending energy index	
	40	0.0261	65.632	

activity during the second sighting; the "11.23" impact (⑤) during the impact appears without obvious abnormalities, indicating that the impact appears unrelated to the roof activity and is expected to be affected by the superimposed disturbance of the stopping coal column and small fault at the No. 704 working face [12].

3. Mechanism Analysis of Impact

As the No. 705 fully mechanized top coal caving face did not appear as obvious mine pressure, dynamic pressure power appears, but during the recovery period occurred, 5 serious impacts appear, and the location of the appear mainly

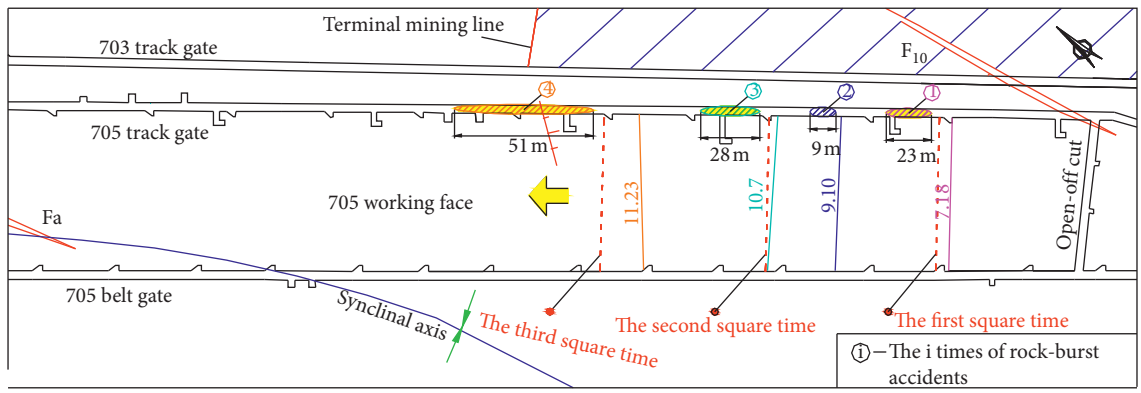

Figure 2: Relation between the position of No. 705 working face and the corresponding 5 times rock burst records.

concentrated in the working face ending over the front working face within a certain range. After the excavation of the roadway, the original three-way stress state of the underground coal-rock body is redistributed and the stress concentration formed in the coal-rock body of the two gangs of the roadway is not enough to induce the impact appearing accident. When the No. 705 fully mechanized top coal caving face is retrieved, the lateral residual support pressure of the adjacent mining area and the superfront support pressure of this working face are superimposed, and it is easy to form a high concentrated static load in the L-shaped area of the superfront section of the No. 705 return air channel, and the stress superimposed value is highest at the convex corner of the L-shaped area. The coal pillar body at the convex corner of the L-shaped area is subjected to a high static load with a stress concentration factor of n. Consider that the coal body around the pillar body has a certain lateral enclosing pressure effect on it. Therefore, the coal pillar is in a triaxial stress state and cannot be simply analyzed by uniaxial compression. The superimposed support pressure of the coal pillar in the L-shaped area is shown in Figure 3(a) [13].

According to the concept of "internal and external stress field" of support pressure from Figure 3(b), it can be seen that, with the back mining of the No. 705 comprehensive workings, the low rock layer instantly breaks the movement and forms a stable structure, and the low rock weight shifts to the coal body and the side of the mining area, forming a lower stress peak $K_2\gamma H$ within the solid coal gang. Due to the hysteresis breaking effect of the high-level rock layer, it lags the low-level rock layer by a certain time to break to form a stable structure, and the high-level rock weight is transferred to the coal body and the deep side of the mining area. From Figure 3, it can be seen that the stress concentration caused within the solid coal gang after the formation of stable structure in the low rock layer and the superposition of over-supporting pressure at the working face form a higher stress peak $n\gamma H$ ($n > K_2$), at which time the coal pillar at the convex corner of the L-shaped area is affected by the action of a higher concentrated static load.

According to *Mohr–Coulomb* strength criterion [14, 15], the ultimate compressive strength of coal pillar under triaxial stress state is as follows:

$$\sigma_{\max} = 2C\frac{\cos\phi}{1-\sin\phi} + \frac{1+\sin\phi}{1-\sin\phi}\sigma_3, \tag{1}$$

where $\sigma_{\max}$ is the ultimate principal stress, σ_3 is the lateral circumferential pressure, C is the cohesion, and φ is the angle of internal friction.

When the coal pillar is under lateral confining pressure, $\sigma_3 = 0$ MPa, and the uniaxial resistance pressure is as follows:

$$R_c = 2C\frac{\cos\phi}{1-\sin\phi}. \tag{2}$$

Using the trigonometric constant equation,

$$\frac{1+\sin\phi}{1-\sin\phi} = \tan^2\left(\frac{\pi}{4}+\frac{\phi}{2}\right) = \tan^2\theta, \tag{3}$$

where θ is the shear breaking angle of coal pillar.

Then, the load required for the instability failure of coal pillar should meet the following requirements:

$$\sigma \geq \sigma_{\max} = R_c + \sigma_3\tan^2\theta. \tag{4}$$

Equation (4) shows that the load required for destabilization of the coal pillar increases proportionally with the increase in lateral circumferential pressure for a certain shear break angle.

Under a certain lateral confining pressure, the elastic strain energy accumulated before failure is higher than that under zero confining pressure, which will release more elastic energy and cause more severe damage to the roadway. The coal pillar at the convex corner of the L-shaped area of the roadway is subject to the superposition of the support pressure and is in a higher state of concentrated static load, and the dynamic load caused by the mining activity of No. 705 working face is superimposed with it, which is prone to two types of typical impact ground pressure of the pressure type and impact (pressure) type of the roadway gang [16], as shown in Figure 4.

As can be seen from Figure 4, the No. 705 working face back mining causes dynamic disturbances such as roof rupture, breakage, or fault slip destabilization, which easily causes the coal pillar to be affected by the superposition of dynamic and static load disturbance. When the working face advances to the first "square" and multiple "square" position,

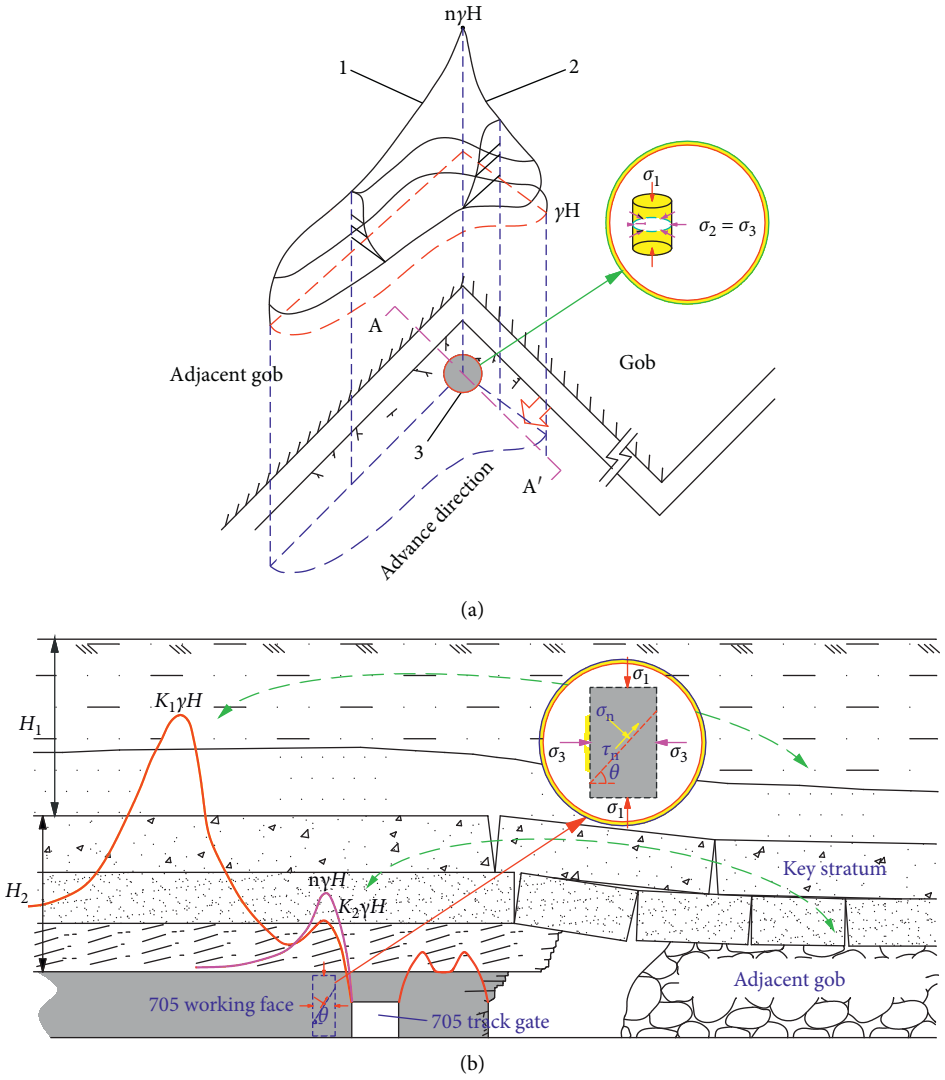

Figure 3: Simplified model of the coal pillar in L-shaped zone: (a) superimposed support pressure of the coal pillar in the L-shaped area; (b) A-A′ section.

the hard roof is very easy to appear "O-X" broken across the fall, resulting in violent power disturbance, increasing the chance of coal pillar destabilization damage impact appearing and impact strength.

The above analysis explains that the occurrence of the ①, ②, and ④ mine pressure dynamic appearances in Figure 2 is directly related to the superimposed dynamic and static load disturbance at the convex corner of the L-shaped area at the end of the working face from a mechanical mechanism perspective. Also, the ① and ④ impacts appeared the most serious because, at this time, the working surface is in the primary and secondary square positions.

The occurrence of each impact display is basically accompanied by the appearance of the bottom drum, which is because after the tunnel is dug out and stabilized, the horizontal stress in the surrounding rock is transferred to the top and bottom plate, resulting in the bottom plate subjected to a certain strength of the horizontal stress σ_x, so that the bottom plate is damaged by a certain degree of flexural deformation. Under the action of superimposed disturbance of high concentrated static load of the roadway gang and dynamic load of the working face retrieval, the coal pillar is prone to produce impact slip along the slip line according to the Terzaghi theory [17], resulting in instantaneous violent bottom drum, and in severe cases, the coal body rushes into the roadway to form impact ground pressure. The influence of the coal pillar on the damage of the roadway floor under the superposition of dynamic and static load disturbance conditions is shown in Figure 5.

There is no abnormality in the mine pressure data during the ⑤ power manifestation in Figure 2, which indicates that the coal pillar at the convex corner of the L-shaped area in front of the working face is not affected by the dynamic disturbance of the roof activity. It can be seen from the figure that, at this time, there is a small fault with a drop of 3.5 m in front of the working face, and the overrun support pressure of the working face is superimposed with the fault support pressure to form a support pressure with a stress peak of

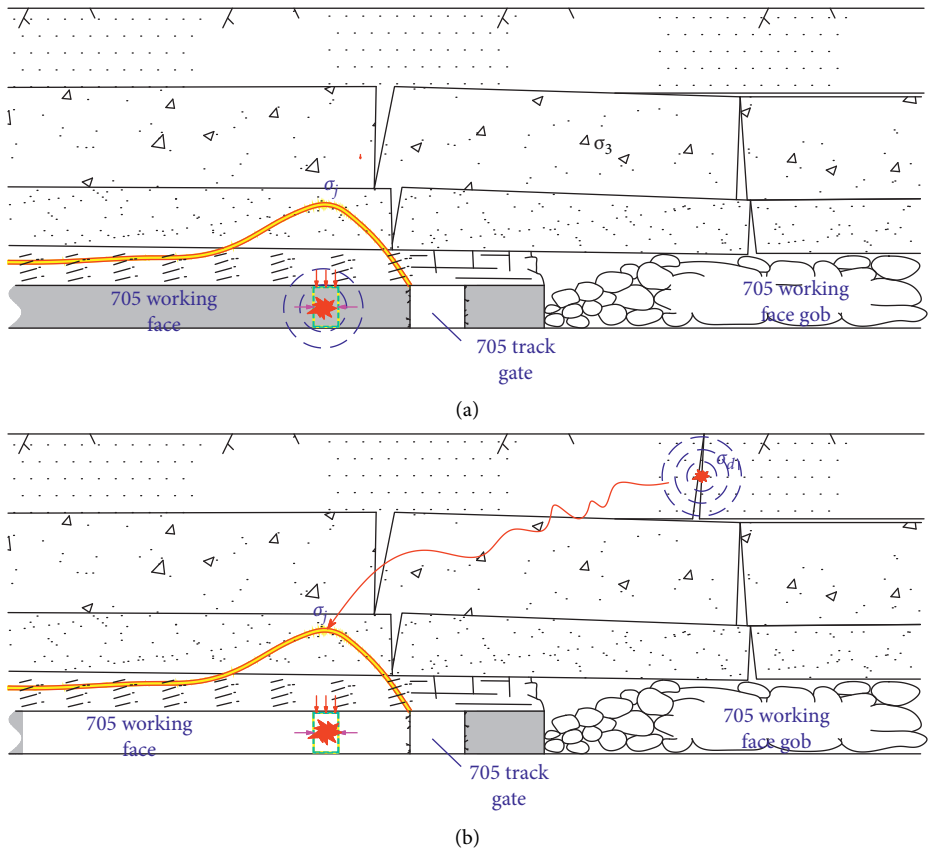

Figure 4: Typical rock burst in roadways: (a) pressure type; (b) impact type.

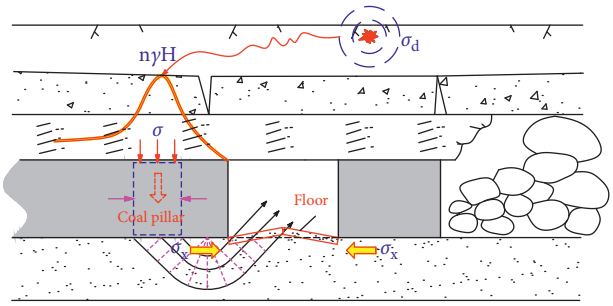

Figure 5: Simplified model of floor rock burst.

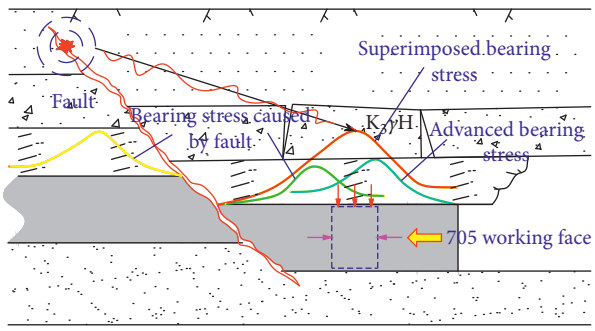

Figure 6: Simplified model of No. 705 working face going through faults.

$K_3\gamma H$, combined with Figure 3(a), which is then superimposed with the lateral support pressure to form a support pressure with a stress peak of $n_1\gamma H$ at the convex corner of the L-shaped area ($n_1 > n$). At the same time, when the working face advances to the vicinity of the small fault, the fault structure is induced to activate the release of dynamic load, and the coal pillar is also affected by the strong dynamic and static load superposition disturbance (dynamic load source is the small fault), and it is very easy to destabilize and damage the roadway impact accident, as in Figure 6.

4. Mechanical Response of the Coal Column under Superimposed Dynamic and Static Load Disturbance

In the deep mining process, it is based on the principle of superimposed dynamic and static load disturbance, and the coal body is susceptible to superimposed disturbance of static and dynamic load source fields. Static loads are mainly composed of self-weight stresses, tectonic stresses, and the mining support pressures developed during the mining process. Dynamic loads are mainly caused by the rupture, breakage, or fault slip destabilization of the coal-rock body causing the elastic energy accumulated in the coal-rock body to be released into the surrounding space in the form of vibratory stress waves, thus creating a dynamic disturbance to the propagating medium. Since the forces are directional,

the dynamic and static loads act on the coal-rock body in the form of vectors, and the superposition of dynamic and static loads on the coal-rock body can be expressed as follows [18]:

$$\sigma_{jd} = \left|\vec{\sigma}_j + \vec{\sigma}_d\right|, \tag{5}$$

where $\vec{\sigma}_j$ is the static load force source field, $\vec{\sigma}_i$ is the dynamic load force source field, and σ_{jd} is the superposition of dynamic and static loads.

It is assumed that the critical value of coal-rock body around mining space-induced rock burst is about $\sigma_{\min}$, and it means that when the inequality meets the following conditions, rock burst will occur:

$$\sigma_{jd} \geq \sigma_{\min}. \tag{6}$$

4.1. FLAC^{3D} Numerical Calculation Model. FLAC^{3D} numerical simulation software has 11 simulated material intrinsic models to choose from. The correct and reasonable choice of material similar intrinsic models is a key factor in 3D numerical calculation and analysis [19]. The commonly chosen instantonal models for coal-rock bodies can be broadly classified into four typical instantonal models: pure elastic (Figure 7(a)), ideal elastic-plastic (Figure 7(b)), elastic-brittle-plastic (Figure 7(c)), and strain-softening (Figure 7(d)), and the simplified stress-strain curves of the four typical instantonal models are shown in Figure 7.

During the deep shaft mining process, the coal column near the extraction space is subjected to a certain amount of lateral envelope pressure. Unlike under zero envelope pressure conditions where the coal column is damaged in a brittle manner along a single oblique shear rupture surface, as the lateral envelope pressure increases, the stress-strain curve of the coal column will reflect the curve characteristics, as shown in Figure 8. The stress-strain curve in Figure 8 comprises an elastic characteristic interval where the strain is small and reversible and a nonlinear characteristic interval where internal damage to the coal body occurs resulting in permanent deformation.

Based on the above analysis of the stress and stress-strain curves of the coal column near the extraction space, it can be seen that the three elastoplastic instantonal models in Figures 7(a)–7(c) ignore the strength softening characteristics of the material and are not well suited to the 3D numerical simulation study of the coal column near the extraction space, while the strain-softening model in Figure 7(d) can well reflect the real stress-strain state of the coal pillar under engineering conditions and can meet the numerical simulation study of the coal column with certain surrounding pressure conditions.

Due to the influence of mining activities, the coal body in a certain range around the extraction space is damaged, and the coal body is of poor quality and in the residual strength zone; the coal body far away from the deep part of the extraction space is basically in the original rock stress state, and the coal body is of good quality and in the elastic zone; the coal body in the excessive zone between the residual strength zone and the original rock stress zone is of medium quality, and the coal body here is in the plastic softening zone; if simplified into a coal body column to see, its surrounding is affected by certain strength surrounding pressure, and its stress-strain curve change pattern is similar to Figure 8.

4.2. Strain-Softening Model Calculation and Analysis. The strain-softening model in FLAC^{3D} is an ontogenetic model based on the *Mohr–Coulomb* yield criterion, which is not associated with the shear flow law but with the tension flow law. In the elastic phase, the strain-softening model has exactly the same stress-strain curve as the *Mohr–Coulomb* model, which is commonly used to simulate coal bodies. The difference between the two models is that, after the onset of plastic yielding, the *Mohr–Coulomb* model material cannot reflect the softening effect of the surrounding rock during the plastic yielding phase because the parameters are preset as constants, whereas the cohesion, internal friction angle, shear expansion angle, and tensile strength of the strain-softening model material all decay with the onset of plastic yielding strain. The strain-softening model allows the user to simulate the stress-strain curve during the plastic yielding phase of the material by customising the function of the change in material parameters after plastic yielding.

The average stress-strain curve of the coal sample for three groups, as determined by laboratory physical and mechanical parameters, is shown in Figure 9, with a uniaxial compressive strength of approximately 27.12 MPa, reaching a peak point at a strain of approximately 0.1.

As the strain-softened material parameters decay after plastic yielding as the plastic yielding strain progresses, the uniaxial compression simulation of coal columns using the strain-softened intrinsic model requires the reassignment of material parameters after the peak of the stress-strain curve so that they still have a certain residual strength after the peak damage. The iterative assignment of the cohesion, friction angle, and shear expansion angle parameters after the peak stress is compared with the measured physical parameters of the coal sample and the adjustment of the parameters to determine reasonable parameter values and iteration laws by a trial-and-error method. The error between the peak uniaxial compressive strength value of 27.44 MPa and the measured value of 27.12 MPa does not exceed 5%. After the peak, the experimental test curve showed a sharp decrease in the bearing capacity due to the destabilization of the coal sample, while the strain-softened model still had a certain bearing capacity, which was in line with the uniaxial compression under certain circumferential pressure conditions. The finalised strain-softened model of the coal pillar showed the changes in parameters after the peak, as shown in Table 5.

4.3. Simulation and Analysis of Coal Column Bodies Subjected to Dynamic and Static Superimposed Disturbances. In order to study the impact damage law of the coal pillar body caused by the superimposed dynamic loads such as roof rupture, fracture, or fault slip instability, the stress-strain law of the coal pillar body under the superimposed dynamic and static

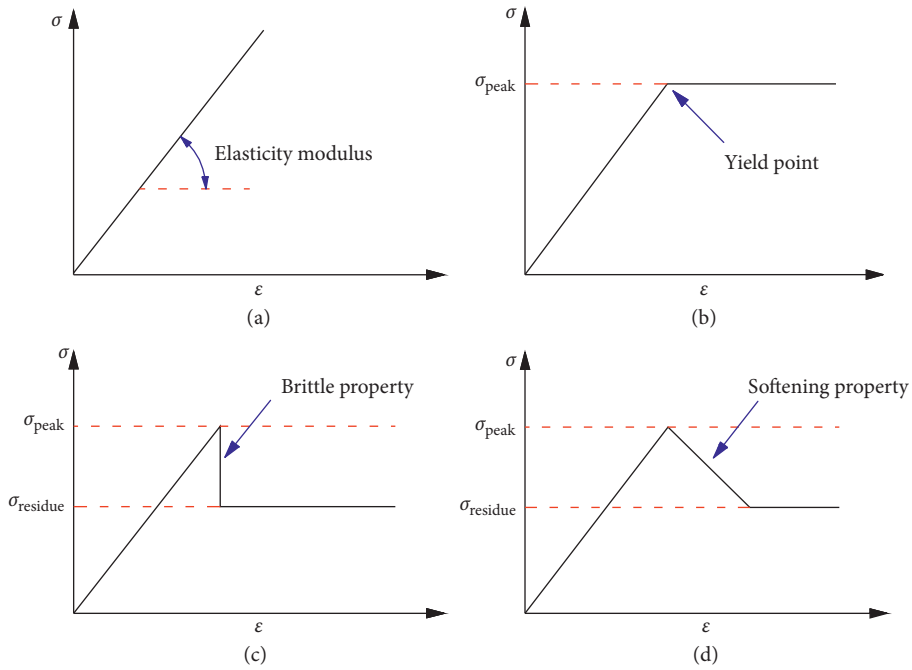

Figure 7: Four simplified intrinsic structure models commonly used for coal bodies: (a) pure elasticity; (b) ideal elasticity; (c) elasticity and brittleness; (d) strain softening.

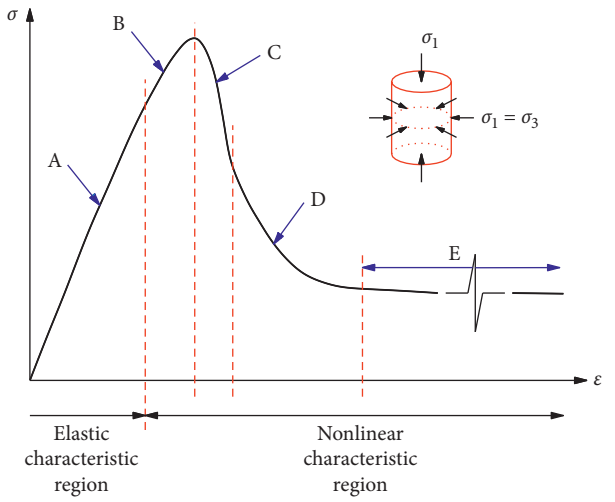

Figure 8: Typical compressive stress-strain curve of rock under certain confining pressure condition. A, linear elastic case; B, prepeak nonlinear phase; C, brittle properties; D, softening properties; E, residual strength.

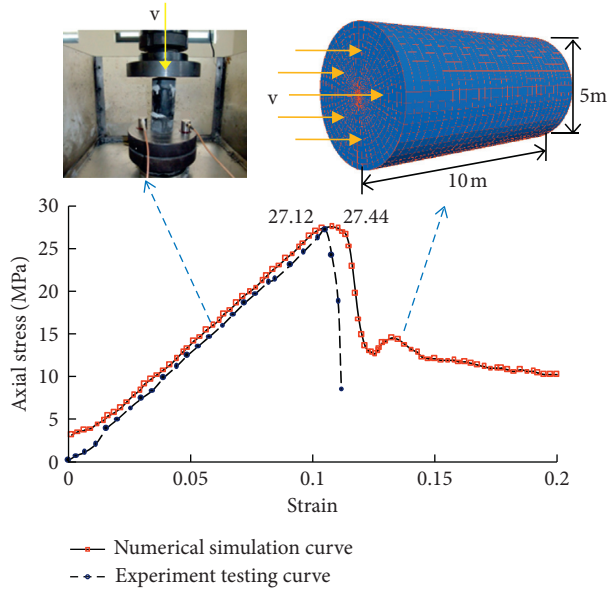

Figure 9: Stress-strain curves of numerical simulation and experimental test.

load disturbance under certain circumferential pressure conditions was investigated by numerical simulation. Statistical studies show that the strain rate of dynamic loads caused by coal mining activities is generally no greater than 10^{-1}/s, which is in the category of medium and medium-low strain rates [15], as shown in Table 6.

A strain-softened model with dimensions of Φ5 m×10 m was built to scale according to the FLAC^{3D} software to simulate a coal column surrounded by certain strength of compression, with the model parameters assigned, as shown in Table 5. A certain value of displacement loading rate was applied to the upper and lower surfaces of the cylinder model to simulate dynamic and static loads.

Under the same static loading conditions, a loading rate of 0.006 m/min was applied to the end face of the strain-softened model, corresponding to a strain rate of 1.0×10^{-5}/s (static load), and when loaded to 20% R_c (5.49 MPa), the loading rate on the end face of the model was varied and loaded at rates of 0.06 m/min, 0.6 m/min, and 3 m/min, respectively, corresponding to the strain rates 1.0×10^{-4}/s (quasidynamic loading), 1.0×10^{-3}/s (dynamic loading), and

Table 5: Mechanical parameters of strain-softening model.

Strain	Cohesion (MPa)	Friction angle (°)	Dilation angle (°)
0	1.3	23	0
0.1	1.3	23	0
0.12	1.0	18	5
0.15	0.7	16	8
0.2	0.6	15	8
1	0.6	15	10

Table 6: Relationship between load and strain rate.

Strain rate (s^{-1})	Change rate of load (MPajingtai)	Type
$<10^{-5}$	<0.1	Static load
10^{-5}~10^{-3}	0.1–10	Stress disturbance
$>10^{-3}$	>10	Dynamic load

5.0×10^{-3}/s (dynamic loading). The numerically simulated stress-strain curves for the coal pillar are shown in Figure 10(a).

Under different static loading conditions, a loading rate of 0.006 m/min was still applied to the strain-softened model end face, and when loaded to 20% R_c (5.49 MPa), 40% R_c (10.98 MPa), 60% R_c (16.46 MPa), and 80% R_c (21.95 MPa), the loading rate to the model end face was changed and both were loaded, respectively. The same loading rate of 0.6 m/min corresponds to a strain rate of 1.0×10^{-3}/s (dynamic load). The numerically simulated stress-strain curves for the coal pillar are shown in Figure 10(b).

From Figure 10(a), it can be seen that the peak stress of the coal column model increases significantly with increasing loading strain rate when the coal column is under the same initial static load, indicating that a larger strain rate enables the coal column to accumulate more elastic strain energy before the peak point. Combined with Figure 10(c), as the strain rate increases, the peak stress of the coal pillar can be reached at a smaller strain, and the slope of the peak stress-strain curve increases as the strain decreases, indicating that a high strain rate can make the coal pillar accumulate more elastic strain energy in a shorter time and smaller strain, which is more likely to induce instability damage of the coal pillar.

From Figure 10(b), it can be seen that the peak stress value increases significantly with the increase in the initial static load of the coal column at the same loading strain rate of 1.0×10^{-3}/s (dynamic load), indicating that a higher initial static load value can make the coal column accumulate more elastic strain energy before the peak point. The slope of the stress-strain curve at the peak point increases sharply with the increase in the initial static load, indicating that the coal pillar in the initial high static load state can accumulate more elastic strain energy in a shorter period of time when disturbed by the loaded dynamic load, which can easily induce the instability of the coal pillar.

The compressive strength of the coal pillar is an important indicator of its propensity to impact. Many scholars have studied the relationship between strength of coal pillar and C_1, and the research results show that when its compressive strength $R_c > 20$ MPa, the minimum critical load $C_1 = 50$ MPa is required for impact to occur, and conversely, when its compressive strength $R_c < 16$ MPa, the critical load $C_1 = 70$–90 MPa is required for impact to occur, as shown in Figure 11.

According to the stress-strain curve in Figure 10(a), combined with Figure 11, it can be seen that when the coal pillar is subjected to a loading strain rate of 5.0×10^{-3}/s (dynamic load) at an initial low static load (20% R_c), the corresponding dynamic and static load superimposed peak strength can reach 63.5 MPa, considering that the uniaxial compressive strength of the coal pillar is 27.44 MPa, which meets the minimum critical load C_1 for impact to occur. When the coal pillar is subjected to low loading strain rate of 1.0×10^{-4}/s (quasidynamic load) and 1.0×10^{-3}/s (dynamic load), its peak strength is less than the value of C_1, so impact damage is not likely to occur.

According to the stress-strain curve in Figure 10(b), combined with Figure 11, it can be seen that when the coal pillar is subjected to the same loading strain rate of 1.0×10^{-3}/s (dynamic load), the peak strength of the dynamic and static load superposition is less than the C_1 value when it is under the initial low static load (20% R_c, 40% R_c) and is less prone to impact damage, while when the coal pillar is under the initial high static load (60% R_c, 80% R_c), its dynamic and static load superposition peak strength is less than the C_1 value. When the coal pillar is under high initial static load (60% R_c, 80% R_c), its dynamic and static load superimposed peak strength meets the condition of the minimum critical load C_1 and is prone to impact damage.

From the above analysis, when the coal pillar is in low static load, it is in low stress yield state, and its own damage requires a large dynamic load perturbation; when the coal pillar is in high static load, it is in high stress yield state, and a smaller dynamic load perturbation can induce the coal pillar instability damage. It can be seen that when the coal pillar is in a low stress yield state, the elastic strain energy required to damage the coal pillar is mainly provided by the external dynamic load, and the dynamic load plays a dominant role in the dynamic and static load superimposed disturbance damage; when the coal pillar is in a high stress yield state, it accumulates a large amount of elastic strain energy, the dynamic load plays a smaller role in the dynamic and static load superimposed disturbance damage than the static load, and the dynamic load mainly plays a role in inducing the damage at this time. Based on the above analysis, measures need to be taken to reduce the concentration of static load strength borne by the coal pillar body, while reducing the strength of the coal pillar body affected by dynamic load disturbance, weakening the dynamic and static load superimposed on the disturbance of the coal pillar body, so as to effectively reduce the chance of the coal pillar body destabilization.

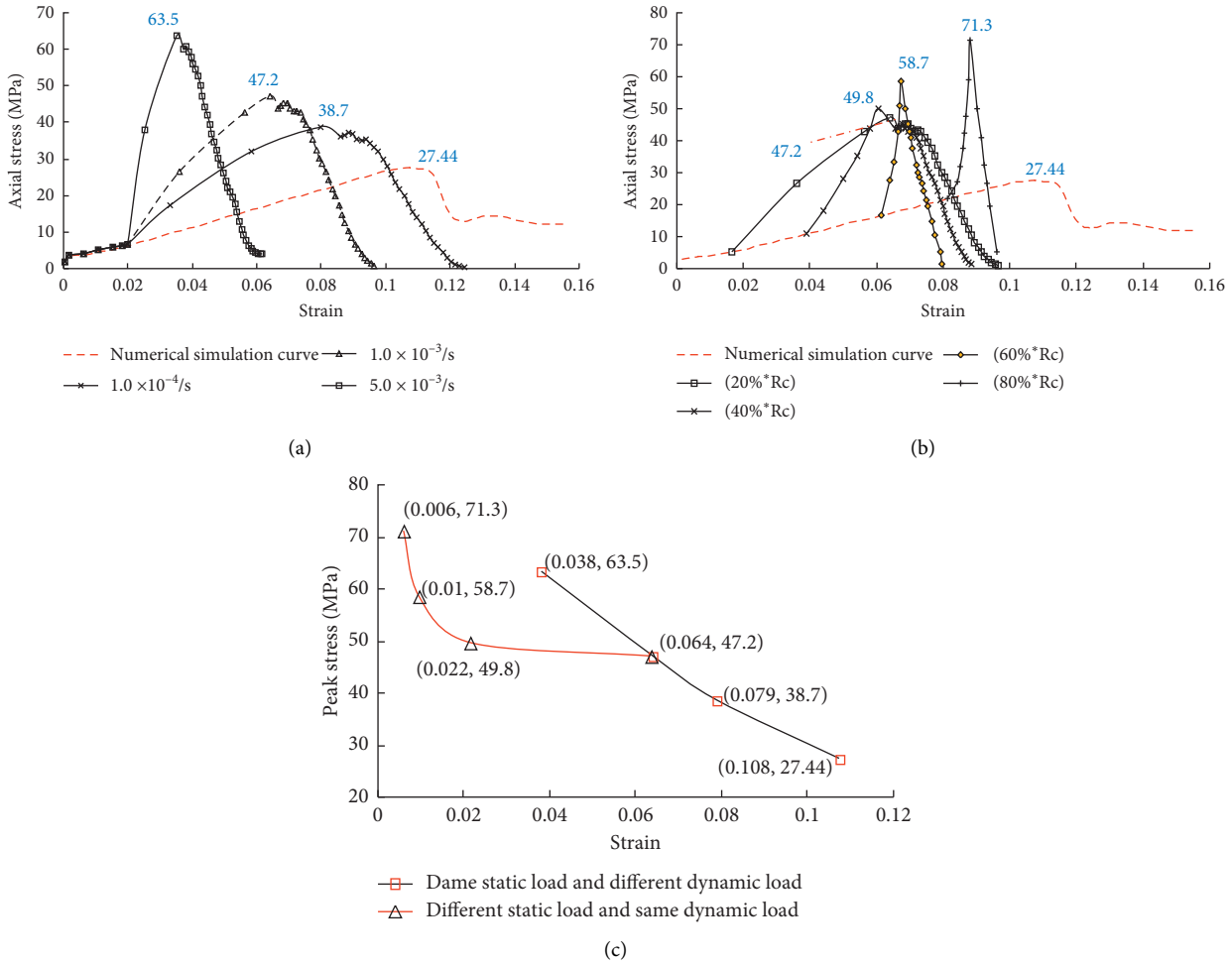

FIGURE 10: Stress-strain curves of coal pillar under dynamic and static combined load: (a) stress-strain curves for superimposed disturbances with the same static load and different dynamic loads; (b) stress-strain curve for superimposed disturbance of the same dynamic load with different static loads; (c) peak point stress-strain curve.

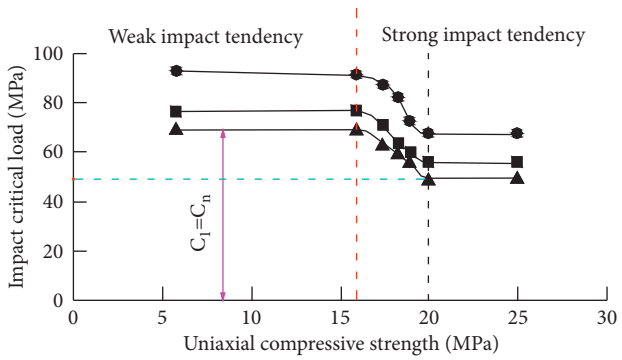

FIGURE 11: Relationship between strength of coal pillar and C_1.

5. Prevention Technology of Rock Burst in L-Shaped Area of Working Face End

5.1. L-Shaped Area Impact Collaborative Control Research. According to the analysis of the mechanical mechanism and numerical simulation results of the coal pillar at the convex corner of the L-shaped area, it can be seen that measures need to be taken to prevent the coal pillar from destabilizing under the action of high concentrated static load and dynamic disturbance to induce impact mine pressure in the roadway and to reduce the strength of high concentrated static load on the coal pillar. At the same time, safe mining technology is adopted to reduce the intensity of the coal pillar affected by dynamic disturbance, thus effectively weakening the degree of dynamic and static load superimposed disturbance on the coal pillar. Combined with the rock burst starting theory put forward by Pan et al., the rock burst of roadway needs to go through three stages: impact starting, impact energy transfer, and impact appearance. Considering the uncertainty and intractable rationality of dynamic disturbance (impact starting) caused by coal mining, from the perspective of impact energy transfer and impact appearance, this paper puts forward some countermeasures for high concentrated static load of coal pillar. High-pressure water jet technology is used to relieve pressure and prevent impact. At the same time, anchor cable is

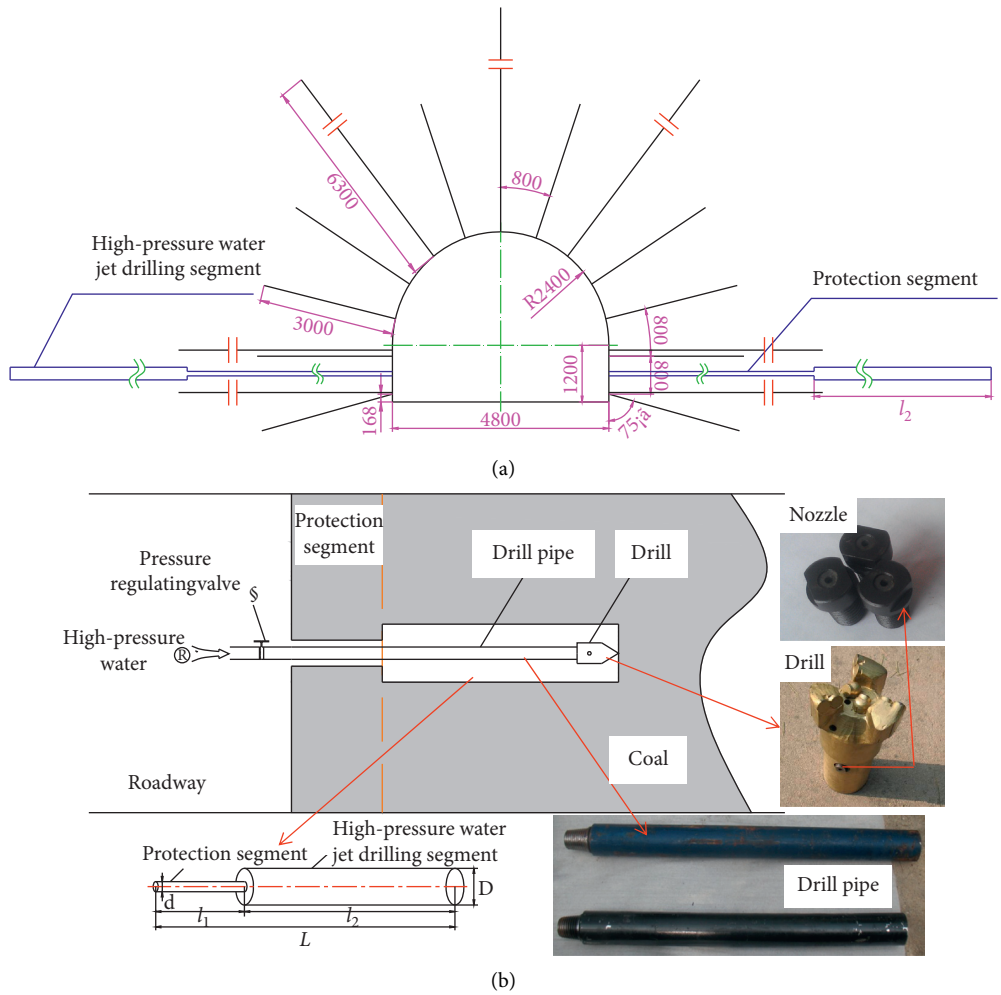

FIGURE 12: Synergistic effect of prevention rock burst: (a) after the high-pressure water jet roadway gang decompression on the basis of cooperative support; (b) schematic diagram of high-pressure water jet roadway gang decompression.

used to strengthen the support of the bolt net supporting structure of the roadway, which has the effect of structural compensation, so as to reduce the damage degree of the impact on the roadway.

The net cross section of the return wind tunnel at No. 705 working face is 4.8 m × 3.6 m. The anchor net is supported by Φ22 × 3000 mm left-handed rebarless rebar anchor rods with 0.8 m × 0.8 m interrow distance. The anchor preload torque is not less than 300 Nm. The anchor cable of secondary gang arch reinforcement support is Φ17.8 × 6300 mm and strength 1860 MPa steel strand, with 400 × 400 mm anchor cable tray, each anchor cable hole should use four Z2350 resin anchorant, and the anchor cable preload is required to be not less than 100 kN. On the basis of the secondary gang arch reinforcement support, high-pressure water jet punching is implemented to unload the coal pillar at the convex corner of the L-shaped area of the roadway gang [20], as shown in Figure 12(a). Among them, high-pressure water jet technology can leave a certain length l_1 of protection zone in the roadway gang and then carry out high-pressure water jet rotary coal cutting on the high stress coal body in the deep part of the roadway gang, using the return water in the hole to discharge the coal body in the cutting area out of the hole and artificially create a certain length l_2 of large diameter pressure relief space (water jet section), as in Figure 12(b).

According to the engineering geological conditions of 705 working face, the simulation study of anchor net support and anchor cable net support was carried out by applying FLAC^{2D} numerical simulation software, and the simulation results are shown in Figures 13(a) and 13(b). From the stress cloud Figure 13(a), it can be seen that the thickness of the compression arch formed by the anchor network support is nearly 1.5 m, and the compressive stress in the arch is about 7.5×10^4 Pa. From the stress cloud (Figure 13(b)), it can be seen that, after compensating for the reinforced support of the gang arch, the anchor mesh cable synergistic support makes the arch thickness increase to 3 m, and the compressive stress in the combined arch increases to about 1.0×10^5 Pa. It can be seen that, after the structural compensation of the original anchor mesh support structure of 705 return wind chute, the anchor mesh rope synergistic support structure has greatly improved the bearing capacity of the roadway surrounding rock and formed a certain range of strong structural area

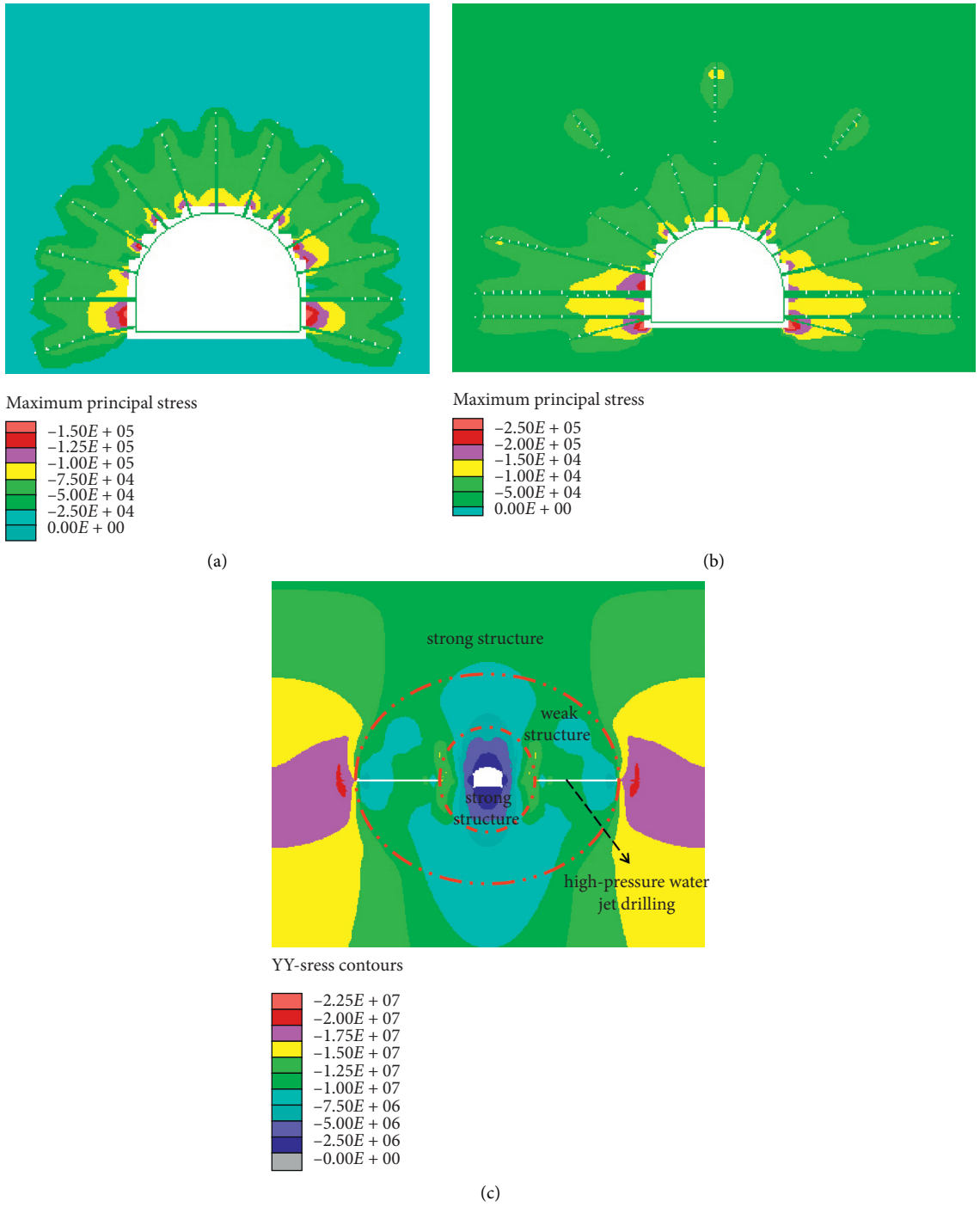

Figure 13: Numerical simulation results: (a) anchor net support; (b) anchor network cable is cooperatively supported; (c) after the high-pressure water jet roadway gang decompression on the basis of cooperative support.

around the roadway. On the basis of the anchor mesh cable synergistic support, a protection belt of length $l_1 = 5$ m is left, and water jet drilling of length $l_2 = 15$ m and diameter $D = 300$ mm is implemented. The stress cloud diagram is shown in Figure 13(c), which shows that the large diameter unloading space formed by the water jet drilling section can cause plastic deformation of the coal body in this area, making the coal body loose and broken, and the strength becomes relatively low. And the porosity is relatively increased, thus effectively releasing and transferring the high concentrated static load in the coal body of the roadway gang, thus forming a certain range of weak structural area. The weak structure area is a large-scale strong structure area which is not affected by mining and basically keeps the original state.

Figure 14(a) shows the distribution of the bending moment carried by the roadway envelope during anchor net support. It is known from the figure that when the ordinary

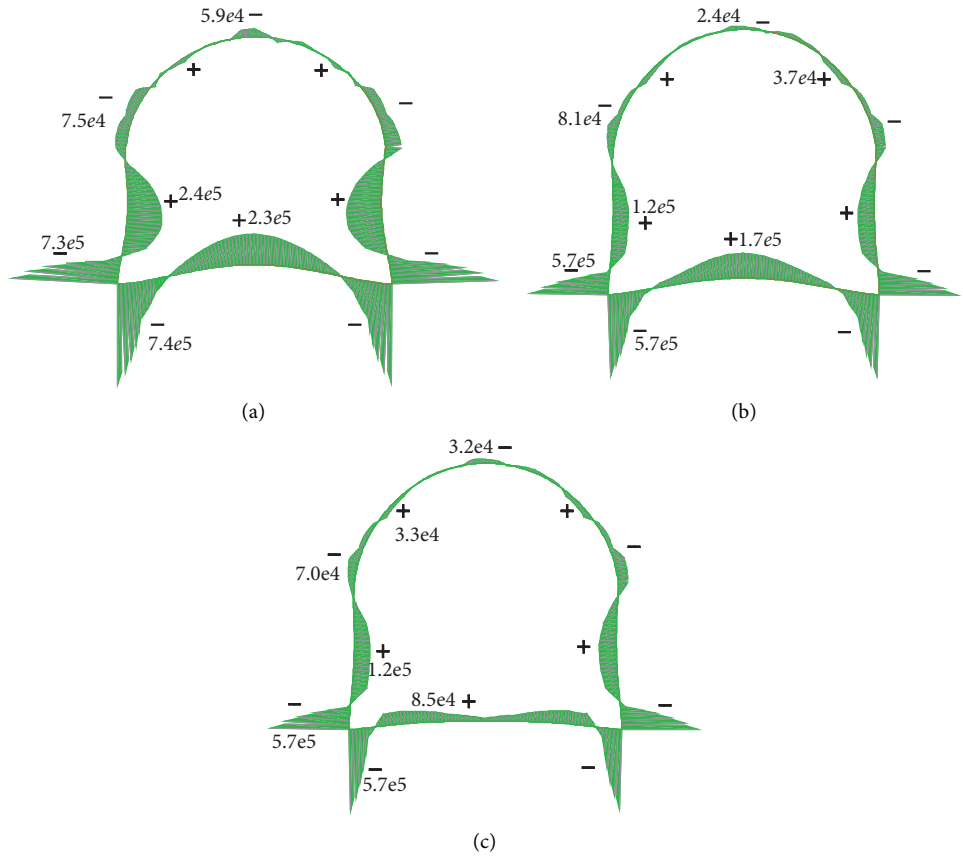

Figure 14: The moment distribution of surrounding rock (unit: Nm): (a) anchor net support; (b) anchor network cable is cooperatively supported; (c) after the high-pressure water jet roadway gang decompression on the basis of cooperative support.

anchor network supports, the two gangs and the bottom plate bending moment is larger, the maximum bending moment in the middle of the two gangs is about 2.4e5 Nm, and the maximum bending moment in the middle of the bottom plate is about 2.3e5 Nm. Figure 14(b) is the distribution of the bending moment carried by the surrounding rock of the roadway when the anchor network cable is cooperatively supported, it is known from the figure that the maximum bending moment in the middle of the two gangs is about 1.2e5 Nm, the maximum bending moment in the middle of the bottom plate is about 1.7e5 Nm, the position in the middle of the gangs drops by 50%, and the position in the middle of the bottom plate drops by 26.1%. Figure 14(c) shows the distribution of the bending moment carried by the surrounding rock of the roadway after the high-pressure water jet roadway gang decompression on the basis of cooperative support. It can be seen that the moment distribution of the bearing structure of the tunnel surrounding rock is more uniform, especially the bottom plate position, due to the role of the unloading of the tunnel gang, the original middle position of the maximum bending moment has been effectively improved, the maximum bending moment of the bottom plate to the two gang feet offset, and the maximum bending moment is about 8.5e4 Nm, which is conducive to the stability of the bottom plate and gang feet surrounding rock.

5.2. Control Effect of Rock Burst. Figure 15 shows the effect before and after the adoption of the prevention and control technology in a mine of Yimei Coal. From Figure 15(b), it can be seen that, for the L-shaped area at the end of the working face, on the basis of the anchor mesh rope support + high-pressure water jet lane gang pressure relief, the U-shaped bracket passive support is applied to the fractured section of the surrounding rock to compensate with it, which can well improve the bearing performance and impact resistance of the lane surrounding rock.

Drill chip method is the most common and effective means to monitor the stress in the roadway surrounding rock. In the follow-up mining process of No. 705 working face, a drilling hole with a diameter of 42 mm can be drilled in the solid coal wall of the superfront section of the return air chute. The stress value in the solid coal wall can be determined by the amount of powder discharged per meter and whether there are dynamic phenomena such as sticking and suction in the drilling process, so as to determine the strength of the impact risk. Combined with the actual production situation of the coal mine, the monitoring of pulverized coal quantity, and the actual appearance of ground pressure, the method of classification prediction and prevention based on the critical index rate value of pulverized coal is preliminarily proposed, as shown in Table 7. The supercritical index rate of pulverized coal can be expressed by

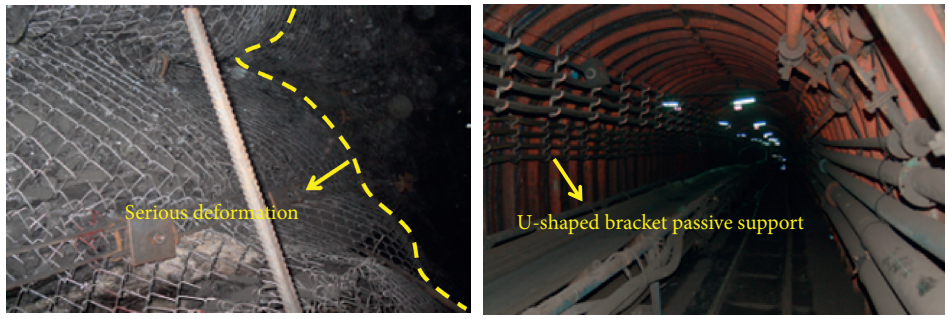

(a) (b)

Figure 15: In situ case of synergistic effect: (a) anchor net support; (b) after the high-pressure water jet roadway gang decompression on the basis of cooperative support.

Table 7: Prediction and prevention method of limit value of coal mines.

Critical index rate of pulverized coal	Pulverized coal		Dangerous state	Prevention method
	1~5 m	5~10 m		
<0	<2.16	<4.86	None	
0–25%	2.16~2.7	4.86~6.1	Weak	Enhancement of monitoring
25%–50%	2.7~3.24	6.1~7.3	Medium	Water injection and pressure relief by large diameter drilling
>50%	>3.24	>7.3	Strong	Cooperative support and pressure relief of the roadway gang

$$I = \frac{m - M}{M} \times 100\%, \tag{7}$$

where I is the critical index rate of pulverized coal, m is the measured pulverized coal quantity, and M is the critical value of pulverized coal quantity.

As shown in Table 7, when the critical index rate $I > 50\%$ of coal dust in the L-shaped area of the overrun section at the end of the No. 705 working face means there is a strong impact hazard, effective prevention and control measures such as cooperative support and pressure relief of the roadway gang need to be taken. Later, according to the prevention and control effect on site, adjust to determine a more suitable coal dust critical index rate grading prediction and prevention method for this working face.

6. Conclusions

(1) The coal pillar at the convex corner of the L-shaped area at the end of the No. 705 working face is subject to high concentrated static load, and the dynamic disturbance caused by mining at the working face makes the coal pillar subject to superimposed dynamic and static load, and its destabilization damage causes pressure type or impact (pressure) type, two types of typical roadway gang, impact ground pressure.

(2) According to the measured stress-strain curve of a coal seam, the strain-softening intrinsic model in FLAC^{3D} software is used to simulate the dynamic characteristics and damage law of the coal pillar under different combinations of dynamic and static loads under certain circumferential pressure conditions, and the mechanical characteristics of the coal pillar are obtained: at low static load, the elastic strain energy required for the damage of the coal pillar is mainly provided by the external dynamic load; at high static load, a large amount of elastic strain energy is accumulated in the coal pillar, and the dynamic load mainly plays the role of inducing damage.

(3) The slope of the strain-peak stress curve of the coal pillar under the same dynamic load conditions with different static loads is significantly greater than that under different dynamic load conditions with the same static load. Under the influence of superposition of dynamic and static loads, the effect of increasing static load on instability damage of coal pillar is higher than that of dynamic load.

(4) Based on the mechanism of impact pressure induced by instability of coal pillar under the condition of superposition of dynamic and static load, the impact pressure prevention and control technology of L-shaped zone at the end of working face is discussed. Anchor mesh rope support and high-pressure water jet roadway gang pressure relief synergy can reduce the high concentration of static load in the L-shaped area of the solid coal gang, the formation of strong and weak-strong triple impacts prevention structure in the roadway envelope, effectively weakens the chance of dynamic and static load superposition-induced impact pressure, and reduces the degree of damage to the roadway by impact manifestation. It is proposed to make graded prediction forecasting and prevention of impact ground pressure based on the magnitude of the critical index rate value of pulverized coal.

Data Availability

All data used to support the findings of this study are included within the article, and there are not any restrictions on data access.

Conflicts of Interest

The authors declare that there are no conflicts of interest.

Acknowledgments

The work was supported by the Engineering Laboratory of Deep Mine Rockburst Disaster Assessment Open Project (LMYK2020005).

References

[1] J. G. Guo, W. G. Wang, Z. Q. Yang et al., "Research of coal pillar inducing rock burst in L-shaped zone of working face and prevention technology," *Journal of Mining Science and Technology*, vol. 2, no. 1, pp. 49–57, 2017.

[2] Z. Yang, C. Liu, S. Tang, L. Dou, and J. Cao, "Rock burst mechanism analysis in an advanced segment of gob-side entry under different dip angles of the seam and prevention technology," *International Journal of Mining Science and Technology*, vol. 28, no. 6, pp. 891–899, 2018.

[3] L. M. Dou and X. Q. He, *Theory and Technology of Rock Burst Prevention*, China University of Mining and Technology Press, Xuzhou, China, 2001.

[4] Y. S. Pan, "Integrated study on compound dynamic disaster of coal-gas outburst and rockburst," *Journal of China Coal Society*, vol. 41, no. 1, pp. 105–112, 2016.

[5] H. He, L. M. Dou, S. Y. Gong et al., "Mechanism of rockburst prevention and supporting control technology in roadways," *Journal of Mining & Safety Engineering*, vol. 27, no. 1, pp. 40–44, 2010.

[6] T. Li, T. T. Mei, G. Q. Li et al., "Mechanism study of coal and gas outburst induced by rockburst in "three-soft" coal seam," *Chinese Journal of Rock Mechanics and Engineering*, vol. 30, no. 6, pp. 1283–1288, 2011.

[7] W. H. Peng and A. H. Lu, "Numerical simulation of layered crack and failure of roadway surrounding rock under the action," *Journal of Mining & Safety Engineering*, vol. 25, no. 2, pp. 213–216, 2008.

[8] Y. Y. Wen, Z. L. Mu, E. B. Yi et al., "The response features of roadway surrounding rock in different hardness coal seams under dynamic disturbance," *Journal of Mining & Safety Engineering*, vol. 30, no. 4, pp. 555–559, 2013.

[9] L. M. Dou, J. He, A. Y. Cao et al., "Rock burst prevention methods based on theory of dynamic and static combined load induced in coal mine," *Journal of China Coal Society*, vol. 40, no. 7, pp. 298–310, 2015.

[10] M. S. Gao, *Study on the Strong-Soft-Strong Structure Control Mechanism of Roadway Subjected to Rock Burst*, China University of Mining and Technology, Xuzhou, China, 2006.

[11] H. P. Kang, J. H. Wang, J. Lin et al., "High pretensioned stress and intensive bolting system and its application to deep roadways," *Journal of China Coal Society*, vol. 32, no. 12, pp. 1233–1238, 2007.

[12] Z. Q. Yang, Z. Zheng, C. Liu et al., "Coal pillar inducing rock burst in L-shaped zone and prevention technology," *Electronic Journal of Geotechnical Engineering*, vol. 22, no. 2, pp. 591–603, 2017.

[13] G. C. Zhang, Z. J. Wen, S. J. Liang et al., "Ground response of a gob-side entry in a longwall panel extracting 17 m-thick coal seam: a case study," *Rock Mechanics and Rock Engineering*, vol. 53, no. 2, pp. 497–516, 2020.

[14] K. Gao, G. D. Qiao, Z. G. Liu et al., "On classification conception of coal and gas outburst mechanism and its application," *Journal of Mining & Safety Engineering*, vol. 36, no. 5, pp. 1043–1051, 2019.

[15] M. B. Wold, L. D. Connell, S. K. Choi et al., "The role of spatial variability in coal seam parameters on gas outburst behaviour during coal mining," *International Journal of Coal Geology*, vol. 75, no. 1, pp. 1–14, 2008.

[16] G. C. Zhang, Y. L. Tan, S. J. Liang et al., "Numerical estimation of suitable gob-side filling wall width in a highly gassy longwall panel," *International Journal of Geomechanics*, vol. 18, no. 8, pp. 1–15, 2018.

[17] G. A. Zhu, L. M. Dou, Z. L. Li et al., "Mining-induced stress changes and rock burst control in a variable-thickness coal seam," *Arabian Journal of Geosciences*, vol. 5, no. 9, pp. 365–376, 2016.

[18] Z. Q. Wang, J. Y. Qiao, C. Wu et al., "Study on mine rock burst prevention and control technology based on gateway layout with negative coal pillars," *Coal Science and Technology*, vol. 47, no. 1, pp. 69–78, 2019.

[19] J. F. Pan, Y. Ning, D. B. Mao et al., "Theory of rock burst start-up during coal mining," *Chinese Journal of Rock Mechanics and Engineering*, vol. 31, no. 3, pp. 586–596, 2012.

[20] Z. Yang, L. Dou, C. Liu, M. Xu, Z. Lei, and Y. Yao, "Application of high-pressure water jet technology and the theory of rock burst control in roadway," *International Journal of Mining Science and Technology*, vol. 26, no. 5, pp. 929–935, 2016.